

Phonons Drive the Topological Phase Transition in Quasi-One-Dimensional Bi_4I_4

Wenjie Hu,^{1,2,*} Jiayi Gong,^{1,3,*} Yuhui Qiu,^{1,2} Lexian Yang,⁴ Jin-Jian Zhou,^{1,2,†} and Yugui Yao^{1,2,‡}

¹*Centre for Quantum Physics, Key Laboratory of Advanced Optoelectronic Quantum Architecture and Measurement (MOE), School of Physics, Beijing Institute of Technology, Beijing 100081, China.*

²*International Center for Quantum Materials, Beijing Institute of Technology, Zhuhai, 519000, China.*

³*College of Physics, Chengdu University of Technology, Chengdu 610059, China*

⁴*State Key Laboratory of Low Dimensional Quantum Physics, Department of Physics, Tsinghua University, Beijing 100084, China*

(Dated: August 26, 2025)

Quasi-one-dimensional bismuth halides offer an exceptional platform for exploring diverse topological phases, yet the nature of the room-temperature topological phase transition in Bi_4I_4 remains unresolved. While theory predicts the high-temperature β -phase to be a strong topological insulator (TI), experiments observe a weak TI. Here we resolve this discrepancy by revealing the critical but previously overlooked role of electron-phonon coupling in driving the topological phase transition. Using our newly developed *ab initio* framework for phonon-induced band renormalization, we show that thermal phonons alone drive β - Bi_4I_4 from the strong TI predicted by static-lattice calculations to a weak TI above ~ 180 K. At temperatures where β - Bi_4I_4 is stable, it is a weak TI with calculated surface states closely match experimental results, thereby reconciling theory with experiment. Our work establishes electron-phonon renormalization as essential for determining topological phases and provides a broadly applicable approach for predicting topological materials at finite temperatures.

Topological insulators (TIs) constitute a remarkable class of quantum materials characterized by symmetry-protected metallic boundary states, offering significant potential for low-power spintronics and fault-tolerant quantum computing [1–4]. Among the various topological materials discovered, the bismuth halide family Bi_4X_4 ($\text{X}=\text{Br}, \text{I}$) stands out as a superior and versatile platform due to its unique quasi-one-dimensional (1D) structure and its ability to host diverse topological phases [5]. This family has attracted substantial interest since the prediction of large-gap quantum spin Hall (QSH) states in monolayer Bi_4Br_4 [6]. The 1D molecular chain architecture of Bi_4X_4 gives rise to naturally occurring, atomically sharp edges that are ideal for detecting and exploiting topological edge states [7, 8]. This advantage enabled the groundbreaking experimental observation of room-temperature QSH edge states in Bi_4Br_4 [9–11]. When these chains stack to form bulk crystals, subtle variations in stacking sequences yield multiple exotic topological phases, including the first experimental realizations of the long-sought weak TI [12–14], higher-order TI [15–18], and three-dimensional QSH insulator [19, 20]. Compositional engineering further enriches the topological landscape, producing tunable phases such as the weak TI phase in $\text{Bi}_4\text{Br}_2\text{I}_2$ [21, 22] and the coalescence of multiple topological orders in $\text{Bi}_4(\text{Br}_{1-x}\text{I}_x)_4$ systems [23].

However, a fundamental discrepancy between theory and experiment persists for Bi_4I_4 . Unlike Bi_4Br_4 , monolayer Bi_4I_4 is predicted to lie near a topological phase boundary [6]. Variations in the stacking of these monolayers give rise to two bulk phases: the low-temperature α -phase and the high-temperature β -phase [24]. Advanced *ab initio* calculations using hybrid functionals or GW corrections consistently predict β - Bi_4I_4 to be a strong TI with Z_2 invariants (1;110) [25, 26], whereas multiple experiments identify it as a weak TI with invariants (0;001) [12–14]. In stark contrast, the same computational approach accurately captures the higher-order TI na-

ture of α - Bi_4I_4 , with calculated surface states agree well with experiments [14, 27]. This contradiction is particularly puzzling given that α - and β - Bi_4I_4 differ primarily in their stacking sequence [15]. The fact that β - Bi_4I_4 is stabilized only at elevated temperatures suggests that finite-temperature effects beyond static-lattice calculations may be essential [28–35].

In this work, we develop an *ab initio* approach to compute phonon-induced band renormalization in β - Bi_4I_4 . We show that thermal phonons alone modify the band gap and induce band inversion as temperature increases, transforming β - Bi_4I_4 from a strong TI, as predicted in static-lattice calculations, to a weak TI above a critical temperature of ~ 180 K. Remarkably, this band inversion is driven by phonon-mediated coupling between band edges and high-energy states far from the gap, indicating that high-energy states could shape low-energy topology via phonon-mediated processes. Furthermore, typically neglected off-diagonal self-energies are critical for re-opening the gap after band inversion and stabilizing the weak TI phase. At temperatures where β - Bi_4I_4 is thermodynamically stable, our calculations predict a weak TI with Z_2 invariants of (0;001) and gapless topological surface states (TSS) in excellent agreement with angle-resolved photoemission spectroscopy (ARPES) measurements. Our work resolves the long-standing discrepancy in β - Bi_4I_4 and provides a practical *ab initio* framework to predict topological electronic structures in narrow-gap materials at finite temperature.

Theory and methodology.—Electronic structure renormalization due to electron-phonon (e-ph) coupling at finite temperature can be calculated using many-body perturbation theory. At the lowest-order, the e-ph self-energy consists of two contributions: the Fan term and the Debye-Waller (DW) term [36–40]:

$$\Sigma_{nn'}(\mathbf{k}, \omega) = \Sigma_{nn'}^{\text{Fan}}(\mathbf{k}, \omega) + \Sigma_{nn'}^{\text{DW}}(\mathbf{k}). \quad (1)$$

Here, n, n' are the band indices, \mathbf{k} is the crystal momentum. The DW self-energy is static, thus independent of frequency

ω . Under the rigid-ion approximation, the DW self-energy including the off-diagonal terms, can be evaluated as [41, 42]:

$$\Sigma_{nn'}^{\text{DW}}(\mathbf{k}) = \frac{1}{N_{\mathbf{q}}} \sum_{\kappa\alpha\alpha'} \frac{e_{\nu\mathbf{q}}^{\kappa\alpha*} e_{\nu\mathbf{q}}^{\kappa\alpha'}}{2\omega_{\nu\mathbf{q}} M_{\kappa}} \mathcal{D}_{nn'}^{\kappa\alpha\alpha'}(\mathbf{k}) (n_{\nu\mathbf{q}} + 1/2), \quad (2)$$

where $\omega_{\nu\mathbf{q}}$ and $e_{\nu\mathbf{q}}$ are the phonon energy and eigenvector, respectively, $n_{\nu\mathbf{q}}$ is the Bose occupation number. $\mathcal{D}_{nn'}^{\kappa\alpha\alpha'}(\mathbf{k}) = i \langle u_{n\mathbf{k}} | [\partial_{\Gamma\kappa\alpha} \hat{v}_{\text{KS}}, \hat{p}_{\alpha'}] | u_{n'\mathbf{k}} \rangle$, where $|u_{n\mathbf{k}}\rangle$ is the periodic part of the electron wavefunction, $\partial_{\Gamma\kappa\alpha} \hat{v}_{\text{KS}}$ is the derivative of the Kohn-Sham (KS) potential \hat{v}_{KS} with respect to the displacement of atom κ (with mass M_{κ}) in the Cartesian direction α with wavevector $\mathbf{q} = \Gamma$, and $\hat{p}_{\alpha'}$ is the momentum operator.

The Fan self-energy is given by $\Sigma^{\text{Fan}} = i\mathbf{G}_0\mathbf{D}_0$, where \mathbf{G}_0 and \mathbf{D}_0 are the non-interacting electron and phonon propagators in matrix notation, respectively. It can be expressed in terms of electron band energy $\varepsilon_{n\mathbf{k}}$ and $\omega_{\nu\mathbf{q}}$ as [39]:

$$\Sigma_{nn'}^{\text{Fan}}(\mathbf{k}, \omega) = \frac{1}{N_{\mathbf{q}}} \sum_m \sum_{\nu\mathbf{q}} g_{mn\nu}(\mathbf{k}, \mathbf{q})^* g_{mn'\nu}(\mathbf{k}, \mathbf{q}) \times \sum_{\pm} \frac{n_{\nu\mathbf{q}} + [1 \pm (2f_{m\mathbf{k}+\mathbf{q}} - 1)]/2}{\omega - \varepsilon_{m\mathbf{k}+\mathbf{q}} \pm \omega_{\nu\mathbf{q}} + i\eta}, \quad (3)$$

where $g_{mn\nu}(\mathbf{k}, \mathbf{q})$ is the e-ph matrix element, η a small broadening, and $f_{m\mathbf{k}+\mathbf{q}}$ the Fermi occupation number.

The renormalized electronic structure is obtained from the total e-ph self-energy. To properly account for the off-diagonal terms of the self-energy, we employ the static Hermitian approximation, which extends the conventional on-the-mass-shell approximation to the off-diagonal case [42, 43]. Within this approximation, the renormalized electron energies are determined by constructing and diagonalizing the corresponding renormalized Hamiltonian:

$$\tilde{H}(\mathbf{k}) = H^0(\mathbf{k}) + \frac{1}{2} [\tilde{\Sigma}(\mathbf{k}) + \tilde{\Sigma}^\dagger(\mathbf{k})], \quad (4)$$

where $H_{nn'}^0(\mathbf{k}) = \varepsilon_{n\mathbf{k}}\delta_{nn'}$ and $\tilde{\Sigma}_{nn'}(\mathbf{k})$ is defined as $[\Sigma_{nn'}(\mathbf{k}, \varepsilon_{n\mathbf{k}}) + \Sigma_{nn'}(\mathbf{k}, \varepsilon_{n'\mathbf{k}})]/2$.

In practical calculations, the summation over band index m in Eq. (3) poses a formidable challenge for converging the Fan self-energy [44], typically requiring thousands of high-energy empty bands. To circumvent this explicit summation, we employ the Sternheimer equation technique [45, 46]. The full band space is partitioned into two subspaces: a finite set of bands near the band gap or Fermi level (lower subspace) and all remaining high-energy bands (upper subspace). The lower-subspace contribution (lower Fan) is computed directly from Eq. (3) with m restricted to the lower-space bands. The upper-subspace contribution (upper Fan) is obtained by solving the linear Sternheimer equation, as detailed in the Supplemental Material (SM) [47].

We calculate the band structures, phonon dispersions, and derivatives of the KS potential $\partial_{q\kappa\alpha} \hat{v}_{\text{KS}}$ within the Perdew-Burke-Ernzerhof generalized gradient approximation (GGA)

of density functional theory (DFT) and density functional perturbation theory (DFPT) using the QUANTUM ESPRESSO package [48, 49]. These quantities are used to evaluate the DW self-energy [Eq. (2)], upper-Fan self-energy [Eq. (S5) in SM [47]], and e-ph matrix elements on coarse \mathbf{k} - and \mathbf{q} -point grids. Wannier interpolation is then employed to obtain e-ph matrix elements on ultrafine grids required to converge the lower-Fan self-energy [50]. For β -Bi₄I₄, we select 48 bands derived from Bi- p and I- p orbitals as the lower subspace (Fig. S1 in SM [47]) and construct corresponding Wannier functions [51, 52].

To efficiently obtain the renormalized band structure at arbitrary \mathbf{k} , we construct the renormalized Hamiltonian in Wannier basis. We first compute and converge the total e-ph self-energy on a coarse \mathbf{k}_c -grid, yielding the renormalized Hamiltonian in the band basis from Eq. (4), which is then transformed to the Wannier basis using the same unitary matrix \mathcal{U} employed in the Wannier function construction:

$$\tilde{H}(\mathbf{R}) = \frac{1}{N_{\mathbf{k}_c}} \sum_{\mathbf{k}_c} e^{-i\mathbf{k}_c \cdot \mathbf{R}} \mathcal{U}^\dagger(\mathbf{k}_c) \tilde{H}(\mathbf{k}_c) \mathcal{U}(\mathbf{k}_c), \quad (5)$$

where \mathbf{R} is the lattice vector. Renormalized band energies within the lower subspace can be efficiently computed from $\tilde{H}(\mathbf{R})$ at negligible cost. Alternatively, one may directly interpolate the DW and Fan self-energies at arbitrary \mathbf{k} using Wannier function and its perturbation theory [46]. We have verified both approaches yield consistent results. In this work, we adopt the former, which is more efficient and facilitates orbital-projected band analysis and surface-state calculations via the surface Green's function method [53].

Band structures from DFT at the GGA-level often lack sufficient accuracy, requiring corrections from advanced methods such as GW, which add an electron-electron (e-e) self-energy. For β -Bi₄I₄, GW corrections or hybrid functionals are required, but DFPT with these methods is computationally prohibitive [54]. To address this, we adopt a recently developed scheme that incorporates the e-e self-energy into e-ph self-energy calculations [55, 56]. Specifically, we perform hybrid-functional (HSE) calculations to obtain the electronic Hamiltonian in the same Wannier basis as used in our GGA calculations [47]; the difference between the HSE and GGA Hamiltonians defines an effective e-e self-energy in the Wannier basis, which is applied to the Fan self-energy via a corrected electron propagator \mathbf{G}_0 , and added to the renormalized Hamiltonian. The above computational framework is implemented in our PERTURBO package [50]. Further details on the methodology are provided in the SM [47].

Static-lattice calculations.—Monolayer Bi₄I₄ is composed of parallel 1D molecular chains running along b -axis, with adjacent chains offset by $b/2$ [Fig. 1(a)]. These monolayers stack along c -axis to form bulk crystals via two distinct patterns: the low-temperature α -phase adopts the AA' -stacking with a double-layer unit cell [Fig. 1(b)], while the metastable β -phase exhibits the simpler A -stacking with a single-layer unit cell [Fig. 1(c)]. β -Bi₄I₄ is thermodynamically stable only above the structural transition temperature $T_P \approx 300$ K and transforms into the α -phase below T_P [24].

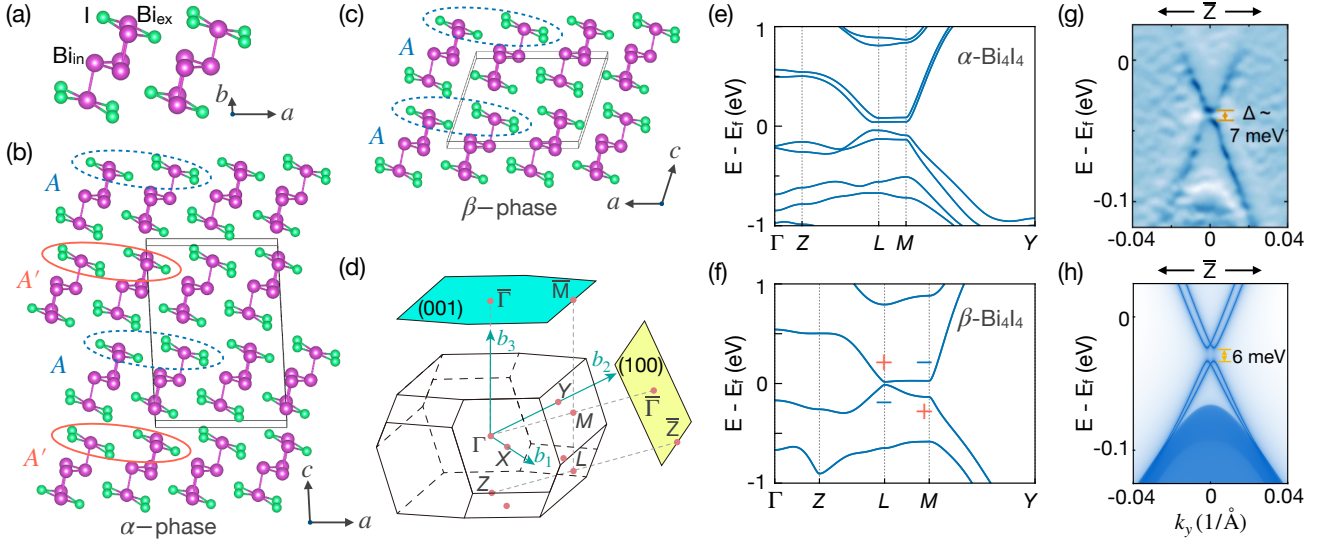


FIG. 1. (a) Conventional unit cell of monolayer Bi_4I_4 . Crystal structures of (b) $\alpha\text{-Bi}_4\text{I}_4$ and (c) $\beta\text{-Bi}_4\text{I}_4$. The A' layer can be viewed as the A layer shifted by one chain along the a -direction. (d) The Brillouin zone of $\beta\text{-Bi}_4\text{I}_4$ and its projections onto the (100) and (001) surfaces. Band structures of (e) $\alpha\text{-Bi}_4\text{I}_4$ and (f) $\beta\text{-Bi}_4\text{I}_4$ from HSE calculations. The \pm symbols in (f) label the parities of bands at L and M points. (g) ARPES spectrum and (h) calculated surface states of the $\alpha\text{-Bi}_4\text{I}_4$ (100) surface. The ARPES spectrum is taken from Ref. [14].

Before incorporating phonon effects, we establish the baseline band structures using static-lattice HSE calculations [47], which also serve as a starting point for subsequent analysis of e-ph renormalization. Figures 1(e) and 1(f) present calculated band structures for α - and β -phase, respectively. For $\alpha\text{-Bi}_4\text{I}_4$, HSE calculations yield excellent agreement with experiment. The computed bulk band gap of ~ 76 meV closely matches the ARPES-measured ~ 85 meV [13]. Calculated surface states [Fig. 1(h), also Fig. S2 in SM [47]] reproduce key features of the ARPES spectrum [Fig. 1(g)], including a surface-state gap of 6 meV versus 7 meV in experiment. Although the calculated Z_2 invariants yield (0;000), $\alpha\text{-Bi}_4\text{I}_4$ hosts topological hinge states characteristic of a higher-order TI (Fig. S3 in SM [47]). This excellent agreement validates our computational approach for the low-temperature phase.

For $\beta\text{-Bi}_4\text{I}_4$, the same methodology predicts a bulk gap of ~ 30 meV and $Z_2 = (1;110)$, indicating a strong TI [Fig. 1(f)]. This result is consistent with previous calculations using GW corrections [26] or hybrid functionals [25]. However, it contradicts experimental evidences pointing to a weak TI [12–14], and the calculated surface states show clear discrepancies with ARPES spectra (see Fig. S4 in SM [47]). This selective failure for the high-temperature β -phase suggests that phonon effects beyond static-lattice calculations may play a critical role.

Phonon-induced topological phase transition.—We incorporate phonon effects into our electronic structure calculations through e-ph self-energy corrections. Figure 2(a) shows the phonon-renormalized band structures of $\beta\text{-Bi}_4\text{I}_4$ at various temperatures. Near the M point, the conduction band shifts upward with increasing temperature, while the valence band remains nearly unchanged. As a result, the local gap increases with temperature, opposite to the temperature-induced

gap narrowing commonly observed in semiconductors. At the L point, the conduction band minimum (CBM) and valence band maximum (VBM) initially move toward each other, leading to an almost closed gap (< 1 meV) at 180 K. The gap reopens upon further heating to 300 K. Figure 2(b) quantifies the temperature dependence of the band gap at the L point. Even at $T = 0$ K, zero-point renormalization reduces the gap from the DFT value of 30 meV to ~ 24 meV. As temperature rises, thermal phonons further suppress the gap until closure near 180 K, the gap then reopens and grows to ~ 36 meV at 400 K. This sequence of gap closure and reopening marks a critical point where band inversion and associated topological phase transition occur.

To confirm the band inversion, we examine the parity and orbital-projected band character of band-edge states across the critical point. At 100 K [Fig. 2(c)], the VBM at the L point with odd parity is dominated by $\text{Bi}_{\text{in}}\text{-}p_x$ character, while the CBM with even parity exhibits mainly $\text{Bi}_{\text{ex}}\text{-}p_x$ character. By 300 K [Fig. 2(d)], both the parities and the orbital characters are reversed, providing definitive evidence of band inversion. As a result, the Z_2 invariants change from (1;110) to (0;001), confirming a topological phase transition from a strong to a weak TI at a critical temperature of ≈ 180 K [Fig. 2(b)].

Importantly, the topological transition temperature lies well below the structural transition temperature of ~ 300 K. This separation of transition temperatures ensures that $\beta\text{-Bi}_4\text{I}_4$ resides exclusively in the weak TI regime under experimentally accessible conditions, as indicated by the shaded region in Fig. 2(b). Notably, this topological phase transition is driven solely by thermal phonons, as all calculations are based on the experimental crystal structure, which exhibits negligible thermal expansion over the relevant temperature range [13]. This

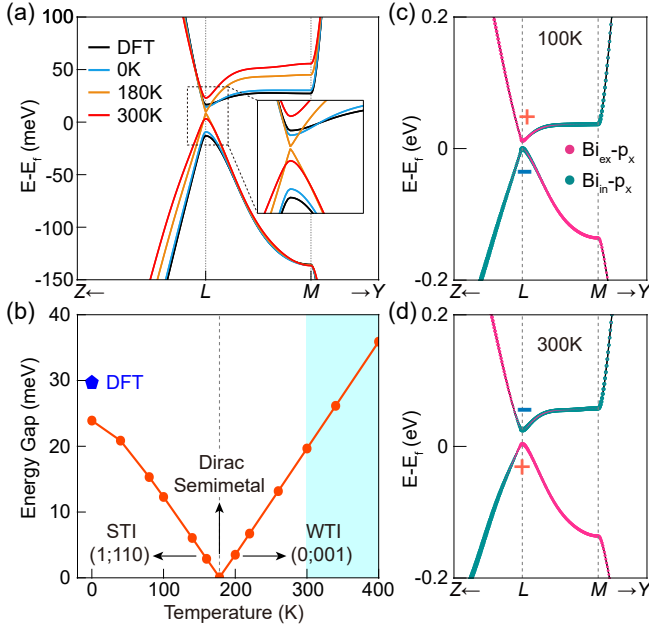


FIG. 2. (a) Phonon-renormalized band structures of β -Bi₄I₄ at different temperatures, with static-lattice DFT result shown for comparison. (b) Temperature-dependent band gap and Z_2 topological invariants. The shaded region indicates the temperature range where β -Bi₄I₄ is thermodynamically stable. The Bi_{in}- p_x and Bi_{ex}- p_x orbital-projected characters of the conduction and valence bands at (c) $T = 100$ K and (d) $T = 300$ K, revealing band inversion near the L point. The \pm symbols label the parities of bands at the L point.

phonon-driven mechanism thus provides the crucial missing link between static-lattice predictions and experimental observations.

We further validate the room-temperature topological phase by comparing calculated surface states with ARPES spectra, as shown in Fig. 3. A key diagnostic for distinguishing the weak and strong TI phases in β -Bi₄I₄ is the presence (absence) of gapless TSS at the \bar{Z} -point (\bar{M} -point) on the (100) side [(001) top] surface [12, 26]. Our calculations predict gapless TSS at the \bar{Z} -point on the (100) surface, exhibiting Dirac-like linear dispersion across the bulk gap [Fig. 3(c)]. The ARPES spectrum shown in Fig. 3(a) reveals similar gapless states. Note that these spectra were obtained using surface-sensitive nano-ARPES [14, 16], which primarily probes surface states and suppresses bulk contributions—explaining the near absence of bulk states features in Fig. 3(a). Equally important, the ARPES spectrum at the \bar{M} -point on the (001) surface shows clearly gapped states [Fig. 3(b)], consistent with our calculation [Fig. 3(d)], which reproduces spectral features of the gapped states with high fidelity. Additional comparisons and the temperature dependence of the calculated surface states are provided in the SM [47]. Taken together, these results provide unambiguous evidence that β -Bi₄I₄ at 300 K is a weak TI with $Z_2 = (0;001)$, and confirm that e-ph renormalization is essential for correctly predicting the topological nature of β -Bi₄I₄.

Finally, we identify two critical mechanisms underlying the

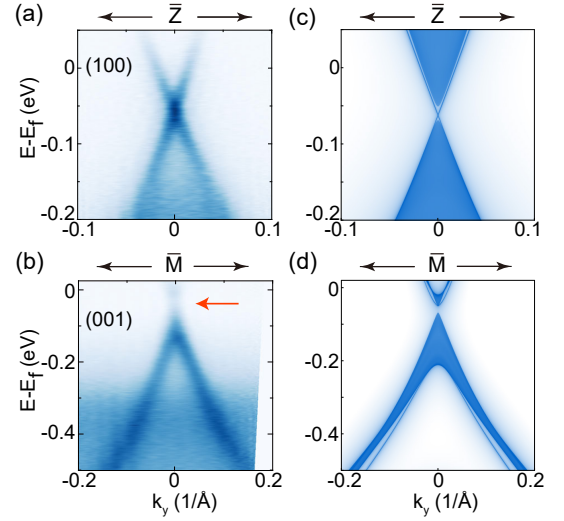


FIG. 3. Comparison between ARPES spectra and calculated surface states of β -Bi₄I₄ at 300 K. ARPES spectra around (a) the \bar{Z} point on the (100) surface and (b) the \bar{M} point on the (001) surface, taken from Ref. [14]. The corresponding calculated surface states on (c) the (100) and (d) the (001) surface.

phonon-driven topological phase transition in β -Bi₄I₄. The first one is phonon-induced wavefunction hybridization enabled by off-diagonal terms of the e-ph self-energy, which allows mixing of near-gap states [42]. Figures 4(a) and 4(b) demonstrate the key role of these off-diagonal terms for reopening the gap after band inversion. At 100 K (before inversion), band structures with and without these terms are nearly identical, indicating negligible hybridization. At 300 K (after inversion), however, these terms become indispensable: omitting them leaves gapless crossings and a metallic state, whereas including them hybridizes the inverted states, reopens the gap, and stabilizes the weak TI phase. Thus, these off-diagonal self-energies drive the gap-reopening process in this transition.

The second one is that the band inversion is driven entirely by phonon-mediated coupling between band edges and high-energy states far from the gap, namely the upper-subspace contribution to the e-ph self-energy, as illustrated in Fig. 4(c). Like the Fan self-energy, the DW self-energy can be partitioned into lower- and upper-subspace contributions, with the lower subspace comprising 48 bands spanning from -6 eV to $+4$ eV of the gap (see Fig. S1 in SM [47]). We obtain the lower- and upper-subspace contributions to the total self-energy by summing the respective Fan and DW terms. Figure 4(d) shows the renormalized CBM and VBM energies as a function of temperature, using only the lower part, upper part, and total self-energy. The lower part produces minor shifts without inversion, whereas the upper part drives substantial shifts and band inversion near 140 K (compared to 180 K for the total). This challenges the conventional wisdom that near-gap states dominate [30], and indicates high-energy states can strongly influence low-energy topology via phonon-mediated processes.

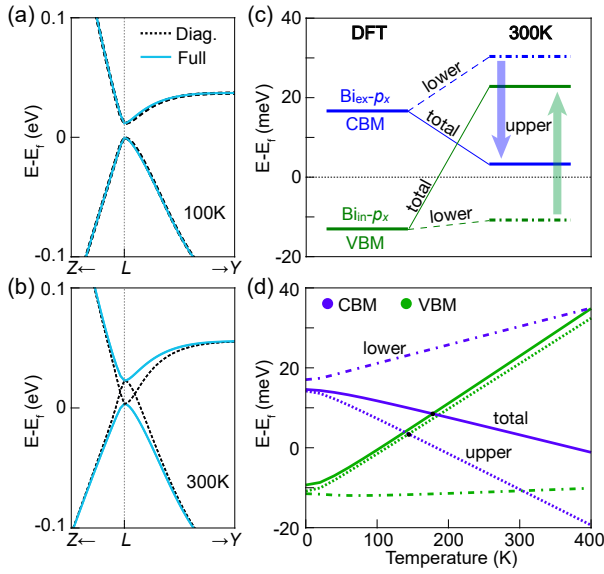


FIG. 4. Phonon-renormalized band structures computed with (solid) and without (dashed) off-diagonal self-energies at (a) $T = 100$ K and (b) $T = 300$ K. (c) Schematic illustration of the renormalized CBM and VBM energies at 300 K, computed with contributions from the lower-subspace only and the total. Arrows highlight the upper-subspace contribution that drives the inversion. (d) The renormalized CBM and VBM energies versus temperature, computed with contributions from only the lower-subspace (dash-dotted), upper-subspace (dotted), and total (solid).

In summary, we resolved the long-standing discrepancy between theory and experiment for the topological phase of β - Bi_4I_4 by identifying e-ph renormalization as the crucial missing ingredient in prior theoretical models. Our results demonstrate that the room-temperature topological phase transition in Bi_4I_4 cannot be explained by structural changes alone, but fundamentally requires temperature-activated phonons, which shape the low-energy topology by mediating coupling to high-energy states. The *ab initio* framework developed here enables accurate finite-temperature predictions, offering both fundamental insights and practical guidance for designing topological materials operating under realistic conditions.

Acknowledgments.—The authors acknowledge support from the National Key R&D Program of China (Grant No. 2022YFA1403400), the National Natural Science Foundation of China (Grant Nos. 12104039, 12321004, 12234003), and the Beijing Natural Science Foundation (Grant No. Z210006).

* W. H. and J. G. contributed equally to this work

† jizhou@bit.edu.cn

‡ ygyao@bit.edu.cn

- [1] M. Z. Hasan and C. L. Kane, Colloquium: Topological insulators, *Rev. Mod. Phys.* **82**, 3045 (2010).
- [2] X.-L. Qi and S.-C. Zhang, Topological insulators and supercon-

ductors, *Rev. Mod. Phys.* **83**, 1057 (2011).

- [3] A. Bansil, H. Lin, and T. Das, Colloquium: Topological band theory, *Rev. Mod. Phys.* **88**, 021004 (2016).
- [4] Y. Ren, Z. Qiao, and Q. Niu, Topological phases in two-dimensional materials: a review, *Rep. Progr. Phys.* **79**, 066501 (2016).
- [5] J. Han, W. Xiao, and Y. Yao, Quasi-one-dimensional topological material Bi_4X_4 ($\text{X}=\text{Br}, \text{I}$), *Adv. Phys.:X* **7**, 2057234 (2022).
- [6] J.-J. Zhou, W. Feng, C.-C. Liu, S. Guan, and Y. Yao, Large-Gap Quantum Spin Hall Insulator in Single Layer Bismuth Monobromide Bi_4Br_4 , *Nano Lett.* **14**, 4767 (2014).
- [7] J.-J. Zhou, W. Feng, G.-B. Liu, and Y. Yao, Topological edge states in single- and multi-layer Bi_4Br_4 , *New J. Phys.* **17**, 015004 (2015).
- [8] J. Han, P. Mao, H. Chen, J.-X. Yin, M. Wang, D. Chen, Y. Li, J. Zheng, X. Zhang, D. Ma, *et al.*, Optical bulk-boundary dichotomy in a quantum spin Hall insulator, *Sci. Bull.* **68**, 417 (2023).
- [9] N. Shumiya, M. S. Hossain, J.-X. Yin, Z. Wang, M. Litskevich, C. Yoon, Y. Li, Y. Yang, Y.-X. Jiang, G. Cheng, *et al.*, Evidence of a room-temperature quantum spin Hall edge state in a higher-order topological insulator, *Nat. Mater.* **21**, 1111 (2022).
- [10] M. Yang, Y. Liu, W. Zhou, C. Liu, D. Mu, Y. Liu, J. Wang, W. Hao, J. Li, J. Zhong, *et al.*, Large-Gap Quantum Spin Hall State and Temperature-Induced Lifshitz Transition in Bi_4Br_4 , *ACS Nano* **16**, 3036 (2022).
- [11] X. Peng, X. Zhang, X. Dong, D. Ma, D. Chen, Y. Li, J. Li, J. Han, Z. Wang, C.-C. Liu, J. Zhou, W. Xiao, and Y. Yao, Observation of Topological Edge States on α - Bi_4Br_4 Nanowires Grown on TiSe_2 Substrates, *J. Phys. Chem. Lett.* **12**, 10465 (2021).
- [12] R. Noguchi, T. Takahashi, K. Kuroda, M. Ochi, T. Shirasawa, M. Sakano, C. Bareille, M. Nakayama, M. D. Watson, K. Yaji, *et al.*, A weak topological insulator state in quasi-one-dimensional bismuth iodide, *Nature* **566**, 518 (2019).
- [13] J. Huang, S. Li, C. Yoon, J. S. Oh, H. Wu, X. Liu, N. Dhale, Y.-F. Zhou, Y. Guo, Y. Zhang, *et al.*, Room-Temperature Topological Phase Transition in Quasi-One-Dimensional Material Bi_4I_4 , *Phys. Rev. X* **11**, 031042 (2021).
- [14] W. X. Zhao, M. Yang, X. Du, Y. D. Li, K. Y. Zhai, Y. Q. Hu, J. F. Han, Y. Huang, Z. K. Liu, Y. G. Yao, *et al.*, Topological phase transition in quasi-one-dimensional bismuth iodide Bi_4I_4 , *npj Quantum Mater.* **9**, 1 (2024).
- [15] R. Noguchi, M. Kobayashi, Z. Jiang, K. Kuroda, T. Takahashi, Z. Xu, D. Lee, M. Hirayama, M. Ochi, T. Shirasawa, *et al.*, Evidence for a higher-order topological insulator in a three-dimensional material built from van der Waals stacking of bismuth-halide chains, *Nat. Mater.* **20**, 473 (2021).
- [16] W. Zhao, M. Yang, R. Xu, X. Du, Y. Li, K. Zhai, C. Peng, D. Pei, H. Gao, Y. Li, *et al.*, Topological electronic structure and spin texture of quasi-one-dimensional higher-order topological insulator Bi_4Br_4 , *Nat. Commun.* **14**, 8089 (2023).
- [17] M. S. Hossain, Q. Zhang, Z. Wang, N. Dhale, W. Liu, M. Litskevich, B. Casas, N. Shumiya, J.-X. Yin, T. A. Cochran, *et al.*, Quantum transport response of topological hinge modes, *Nat. Phys.* **20**, 776 (2024).
- [18] J. Lefeuvre, M. Kobayashi, G. Patriarche, N. Findling, D. Trodec, M. Ferrier, S. Guéron, H. Bouchiat, T. Sasagawa, and R. Deblock, Quantum Coherent Transport of 1D ballistic states in second order topological insulator Bi_4Br_4 (2025), arXiv:2502.13837 [cond-mat].
- [19] S. Yu, J. Deng, W. Liu, Y. Zhang, Y. Sun, N. Dhale, S. Li, W. Ma, Z. Wang, P. Wu, *et al.*, Observation of Robust One-Dimensional Edge Channels in a Three-Dimensional Quantum Spin Hall In-

- ulator, *Phys. Rev. X* **14**, 041048 (2024).
- [20] M. Yang, W. Zhao, D. Mu, Z. Shi, J. Zhong, Y. Li, Y. Liu, J. Zhong, N. Cheng, W. Zhou, *et al.*, Mass Acquisition of Dirac Fermions in Bi_4I_4 by Spontaneous Symmetry Breaking, *Phys. Rev. Lett.* **133**, 256601 (2024).
- [21] J. Zhong, M. Yang, Z. Shi, Y. Li, D. Mu, Y. Liu, N. Cheng, W. Zhao, W. Hao, J. Wang, *et al.*, Towards layer-selective quantum spin hall channels in weak topological insulator $\text{Bi}_4\text{Br}_2\text{I}_2$, *Nat. Commun.* **14**, 4964 (2023).
- [22] R. Noguchi, M. Kobayashi, K. Kawaguchi, W. Yamamori, K. Aido, C. Lin, H. Tanaka, K. Kuroda, A. Harasawa, V. Kandyba, *et al.*, Robust Weak Topological Insulator in the Bismuth Halide $\text{Bi}_4\text{Br}_2\text{I}_2$, *Phys. Rev. Lett.* **133**, 086602 (2024).
- [23] J. Zhong, M. Yang, W. Zhao, K. Zhai, X. Zhen, L. Zhang, D. Mu, Y. Liu, Z. Shi, N. Cheng, *et al.*, Coalescence of multiple topological orders in quasi-one-dimensional bismuth halide chains, *Nat. Commun.* **16**, 1163 (2025).
- [24] C. D. Hinojosa, L. Rodrigues de Faria, G. H. Cassemiro, J. Larrea Jiménez, A. Jefferson da Silva Machado, W. H. Brito, and V. Martelli, Structural investigation of the quasi-one-dimensional topological insulator Bi_4I_4 , *Phys. Rev. B* **109**, 174105 (2024).
- [25] C.-C. Liu, J.-J. Zhou, Y. Yao, and F. Zhang, Weak Topological Insulators and Composite Weyl Semimetals: $\beta\text{-Bi}_4\text{X}_4$ ($\text{X} = \text{Br}, \text{I}$), *Phys. Rev. Lett.* **116**, 066801 (2016).
- [26] G. Autès, A. Isaeva, L. Moreschini, J. C. Johannsen, A. Pisoni, R. Mori, W. Zhang, T. G. Filatova, A. N. Kuznetsov, L. Forró, *et al.*, A novel quasi-one-dimensional topological insulator in bismuth iodide $\beta\text{-Bi}_4\text{I}_4$, *Nat. Mater.* **15**, 154 (2016).
- [27] Y. Liu, R. Chen, Z. Zhang, M. Bockrath, C. N. Lau, Y.-F. Zhou, C. Yoon, S. Li, X. Liu, N. Dhale, *et al.*, Gate-Tunable Transport in Quasi-One-Dimensional $\alpha\text{-Bi}_4\text{I}_4$ Field Effect Transistors, *Nano Lett.* **22**, 1151 (2022).
- [28] I. Garate, Phonon-Induced Topological Transitions and Crossovers in Dirac Materials, *Phys. Rev. Lett.* **110**, 046402 (2013).
- [29] B. Monserrat and D. Vanderbilt, Temperature Effects in the Band Structure of Topological Insulators, *Phys. Rev. Lett.* **117**, 226801 (2016).
- [30] G. Antonius and S. G. Louie, Temperature-Induced Topological Phase Transitions: Promoted versus Suppressed Nontrivial Topology, *Phys. Rev. Lett.* **117**, 246401 (2016).
- [31] J. D. Querales-Flores, P. Aguado-Puente, D. Dangić, J. Cao, P. Chudzinski, T. N. Todorov, M. Grüning, S. Fahy, and I. Savić, Towards temperature-induced topological phase transition in SnTe : A first-principles study, *Phys. Rev. B* **101**, 235206 (2020).
- [32] V. Brousseau-Couture, G. Antonius, and M. Côté, Temperature dependence of the topological phase transition of BiTeI from first principles, *Phys. Rev. Res.* **2**, 023185 (2020).
- [33] T. Imai, J. Chen, K. Kato, K. Kuroda, T. Matsuda, A. Kimura, K. Miyamoto, S. V. Eremin, and T. Okuda, Experimental verification of a temperature-induced topological phase transition in TlBiS_2 and TlBiSe_2 , *Phys. Rev. B* **102**, 125151 (2020).
- [34] F. Giustino, S. G. Louie, and M. L. Cohen, Electron-Phonon Renormalization of the Direct Band Gap of Diamond, *Phys. Rev. Lett.* **105**, 265501 (2010).
- [35] G. Antonius, S. Poncé, P. Boulanger, M. Côté, and X. Gonze, Many-Body Effects on the Zero-Point Renormalization of the Band Structure, *Phys. Rev. Lett.* **112**, 215501 (2014).
- [36] P. B. Allen and V. Heine, Theory of the temperature dependence of electronic band structures, *J. Phys. C: Solid State Phys.* **9**, 2305 (1976).
- [37] P. B. Allen and M. Cardona, Theory of the temperature dependence of the direct gap of germanium, *Phys. Rev. B* **23**, 1495 (1981).
- [38] P. B. Allen and M. Cardona, Temperature dependence of the direct gap of Si and Ge, *Phys. Rev. B* **27**, 4760 (1983).
- [39] F. Giustino, Electron-phonon interactions from first principles, *Rev. Mod. Phys.* **89**, 015003 (2017).
- [40] J. P. Nery, P. B. Allen, G. Antonius, L. Reining, A. Miglio, and X. Gonze, Quasiparticles and phonon satellites in spectral functions of semiconductors and insulators: Cumulants applied to the full first-principles theory and the Fröhlich polaron, *Phys. Rev. B* **97**, 115145 (2018).
- [41] S. Poncé, G. Antonius, Y. Gillet, P. Boulanger, J. Laflamme Janssen, A. Marini, M. Côté, and X. Gonze, Temperature dependence of electronic eigenenergies in the adiabatic harmonic approximation, *Phys. Rev. B* **90**, 214304 (2014).
- [42] J.-M. Lihm and C.-H. Park, Phonon-induced renormalization of electron wave functions, *Phys. Rev. B* **101**, 121102 (2020).
- [43] M. van Schilfgaarde, T. Kotani, and S. Faleev, Quasiparticle self-consistent GW theory, *Phys. Rev. Lett.* **96**, 226402 (2006).
- [44] S. Poncé, J.-M. Lihm, and C.-H. Park, Verification and validation of zero-point electron-phonon renormalization of the bandgap, mass enhancement, and spectral functions, *npj Comput. Mater.* **11**, 117 (2025).
- [45] X. Gonze, P. Boulanger, and M. Côté, Theoretical approaches to the temperature and zero-point motion effects on the electronic band structure, *Ann. Phys.* **523**, 168 (2011).
- [46] J.-M. Lihm and C.-H. Park, Wannier Function Perturbation Theory: Localized Representation and Interpolation of Wave Function Perturbation, *Phys. Rev. X* **11**, 041053 (2021).
- [47] See Supplemental Material at link for details on the computational methods, convergence tests, surface states from HSE static-lattice calculations, calculated hinge states in $\alpha\text{-Bi}_4\text{I}_4$, comparison between calculated surface states and ARPES spectra, and temperature-dependent surface states in $\beta\text{-Bi}_4\text{I}_4$, which includes refs. [57–67].
- [48] P. Giannozzi, S. Baroni, N. Bonini, M. Calandra, R. Car, *et al.*, QUANTUM ESPRESSO: a modular and open-source software project for quantum simulations of materials, *J. Phys.: Condens. Matter* **21**, 395502 (2009).
- [49] P. Giannozzi, O. Andreussi, T. Brumme, O. Bunau, M. Buongiorno Nardelli, *et al.*, Advanced capabilities for materials modelling with Quantum ESPRESSO, *J. Phys. Condens. Matter* **29**, 465901 (2017).
- [50] J.-J. Zhou, J. Park, I.-T. Lu, I. Maliyov, X. Tong, and M. Bernardi, Perturbo: A software package for ab initio electron-phonon interactions, charge transport and ultrafast dynamics, *Comput. Phys. Commun.* **264**, 107970 (2021).
- [51] N. Marzari, A. A. Mostofi, J. R. Yates, I. Souza, and D. Vanderbilt, Maximally localized wannier functions: Theory and applications, *Rev. Mod. Phys.* **84**, 1419 (2012).
- [52] G. Pizzi, V. Vitale, R. Arita, S. Blügel, F. Freimuth, G. Géranton, M. Gibertini, D. Gresch, C. Johnson, T. Koretsune, *et al.*, Wannier90 as a community code: new features and applications, *J. Phys. Condens. Matter* **32**, 165902 (2020).
- [53] M. P. L. Sancho, J. M. L. Sancho, J. M. L. Sancho, and J. Rubio, Highly convergent schemes for the calculation of bulk and surface Green functions, *J. Phys. F: Met. Phys.* **15**, 851 (1985).
- [54] Z. Li, G. Antonius, M. Wu, F. H. da Jornada, and S. G. Louie, Electron-Phonon Coupling from Ab Initio Linear-Response Theory within the GW Method: Correlation-Enhanced Interactions and Superconductivity in $\text{Ba}_{1-x}\text{K}_x\text{BiO}_3$, *Phys. Rev. Lett.* **122**, 186402 (2019).
- [55] D. J. Abramovitch, J.-J. Zhou, J. Mravlje, A. Georges, and M. Bernardi, Combining electron-phonon and dynamical mean-

- field theory calculations of correlated materials: Transport in the correlated metal Sr_2RuO_4 , *Phys. Rev. Mater.* **7**, 093801 (2023).
- [56] D. J. Abramovitch, J. Mravlje, J.-J. Zhou, A. Georges, and M. Bernardi, Respective Roles of Electron-Phonon and Electron-Electron Interactions in the Transport and Quasiparticle Properties of SrVO_3 , *Phys. Rev. Lett.* **133**, 186501 (2024).
- [57] M. van Setten, M. Giantomassi, E. Bousquet, M. Verstraete, D. Hamann, X. Gonze, and G.-M. Rignanese, The PseudoDojo: Training and grading a 85 element optimized norm-conserving pseudopotential table, *Comput. Phys. Commun.* **226**, 39 (2018).
- [58] J. P. Perdew, K. Burke, and M. Ernzerhof, Generalized Gradient Approximation Made Simple, *Phys. Rev. Lett.* **77**, 3865 (1996).
- [59] S. Baroni, S. de Gironcoli, A. Dal Corso, and P. Giannozzi, Phonons and related crystal properties from density-functional perturbation theory, *Rev. Mod. Phys.* **73**, 515 (2001).
- [60] G. Kresse and J. Furthmüller, Efficient iterative schemes for ab initio total-energy calculations using a plane-wave basis set, *Phys. Rev. B* **54**, 11169 (1996).
- [61] G. Kresse and D. Joubert, From ultrasoft pseudopotentials to the projector augmented-wave method, *Phys. Rev. B* **59**, 1758 (1999).
- [62] J. Heyd, G. E. Scuseria, and M. Ernzerhof, Hybrid functionals based on a screened Coulomb potential, *J. Chem. Phys.* **118**, 8207 (2003).
- [63] A. V. Kruckau, O. A. Vydrov, A. F. Izmaylov, and G. E. Scuseria, Influence of the exchange screening parameter on the performance of screened hybrid functionals, *J. Chem. Phys.* **125**, 224106 (2006).
- [64] H. G. von Schnering, H. von Benda, and C. Kalveram, Wismutmonojodid BiI_2 , eine Verbindung mit $\text{Bi}(\text{O})$ und $\text{Bi}(\text{II})$, *Zeitschrift für anorganische und allgemeine Chemie* **438**, 37 (1978).
- [65] F. Giustino, M. L. Cohen, and S. G. Louie, Electron-phonon interaction using Wannier functions, *Phys. Rev. B* **76**, 165108 (2007).
- [66] J. Sjakste, N. Vast, M. Calandra, and F. Mauri, Wannier interpolation of the electron-phonon matrix elements in polar semiconductors: Polar-optical coupling in GaAs, *Phys. Rev. B* **92**, 054307 (2015).
- [67] C. Verdi and F. Giustino, Fröhlich Electron-Phonon Vertex from First Principles, *Phys. Rev. Lett.* **115**, 176401 (2015).